Available online at www.sciencedirect.com

ScienceDirect

Acta Materialia 61 (2013) 6597–6608

Acta MATERIALIA

www.elsevier.com/locate/actamat

How can a minor element added to a binary amorphous alloy simultaneously improve the plasticity and glass-forming ability?

Hong-Kyu Kim [a,1], Mirim Lee [a,1], Kwang-Ryeol Lee [b], Jae-Chul Lee [a,*]

[a] Department of Materials Science and Engineering, Korea University, Seoul 136-701, Republic of Korea
[b] Computational Science Center, Korea Institute of Science and Technology, Seoul 136-791, Republic of Korea

Received 18 June 2013; accepted 23 July 2013
Available online 16 August 2013

Abstract

Minor elements, when added to binary amorphous alloys in small percentages, can often lead to significant improvements in both the plasticity and glass-forming ability (GFA) of the alloys. Considering that plasticity and GFA are two contrasting properties dependent on short-range orders (SROs) of differing degrees, this experimental observation at first seems paradoxical when considered from an SRO viewpoint. In this study, comparative studies on amorphous alloys $Cu_{50}Zr_{50}$ and $Cu_{47.5}Zr_{47.5}Al_5$ were performed using experiments and simulations to elucidate how these two apparently mutually exclusive properties can be realized at the same time. Using molecular dynamics simulations, we resolved the local structures of $Cu_{50}Zr_{50}$ and $Cu_{47.5}Zr_{47.5}Al_5$ in terms of icosahedral medium-range orders. In addition, the role of the minor element (Al) on the formation of the icosahedra and their medium-range structures during cooling, as well as their disordering behavior during subsequent plastic relaxation, was clarified.

Keywords: Amorphous alloy; Short-range order; Medium-range order; Molecular dynamics; Mechanical properties

1. Introduction

In previous studies of the structure–property relationship of amorphous alloys, the atomic-scale structures of the alloys responsible for their measurable macroscopic properties have mostly been analyzed in terms of the degrees of short-range order (SRO) as determined from their fractions, especially those of icosahedra [1–8]. Following experimental and simulation studies [4–9], it is now generally accepted that the higher the fraction of the icosahedral orders (or equivalently, the higher the atomic-packing density) in an amorphous alloy, the higher its glass-forming ability (GFA) and strength [9]. On the other hand, higher plasticity is associated with lower fractions of the icosahedral orders (or lower atomic-packing densities) [5,6]. Therefore, when taking into consideration the SROs, the plasticity and GFA of an alloy are contrasting properties and have their origins in different structures. However, there are some systems in which the dependencies of these properties on the SRO do not hold. According to recent experiments, the addition of a few per cent of minor elements to binary amorphous alloys can often significantly improve both the plasticity and the GFA of the alloys [10–12]. This suggests that any description of the structures of such alloys that only considers SRO and does not take into account the medium-range (or greater) structural hierarchy is not capable of explaining this seemingly contradictory phenomenon of amorphous alloys with a high GFA also exhibiting a large plastic strain.

During cooling, SROs tend to fill the three-dimensional (3-D) space of the amorphous alloys so as to attain the lowest possible energy state [13,14]. This can be achieved by forming a densely packed structure in which the local SROs connect with neighboring ones to form medium-range orders (MROs). Some specific types of MROs in

* Corresponding author. Tel.: +82 2 3290 3283.
E-mail address: jclee001@korea.ac.kr (J.-C. Lee).
[1] These authors contributed equally to this work.

1359-6454/$36.00
http://dx.doi.org/10.1016/j.actamat.2013.07.044

amorphous alloys have been proposed on the basis of model-based studies of efficient packing [15,16]. Several other configurations of MROs have also been identified via an approach that involves both experiments and simulations [16–22]. However, whether these MROs are the major structural components that play a key role in determining the macroscopic properties of the alloys has not yet been established.

Recently, we proposed a conceptual icosahedral MRO termed an "interpenetrating cluster of icosahedra" (ICOI) and attempted to relate its characteristic features to the quantifiable properties of Cu–Zr alloys [14]. Although the results were instructive for identifying the higher level of structural hierarchy beyond SROs that is responsible for the observed properties, the system used in the previous study was a binary one. Considering that most bulk amorphous alloys arise from systems consisting of more than three elements, it is necessary to elucidate whether this conceptual medium-range structure, i.e. the ICOI, can be generically extended to multicomponent alloys and produce self-consistent results even when explaining the contradictory phenomenon mentioned above.

In this study, using experiments and molecular dynamics (MD) simulations of a ternary system, comparative studies on $Cu_{50}Zr_{50}$ and $Cu_{47.5}Zr_{47.5}Al_5$ were performed to explore how and why the minor alloying of $Cu_{50}Zr_{50}$ with Al simultaneously improves both its plasticity and GFA. This was done by elucidating the role of Al in the development of specific types of icosahedral orders and their medium-range structures. We also examined the different roles played by the icosahedra and their medium-range structures from kinetic and dynamic perspectives, in order to quantitatively explain how the mutually exclusive properties of high GFA and large plastic strain are realized.

2. Model alloys and their macroscopic properties

Simple systems provide a valuable testing ground for monitoring the structural changes in amorphous alloys associated with the addition of a minor element and for discussing the effect of these changes on the macroscopic properties of the alloys. The addition of a small amount of Al to $Cu_{50}Zr_{50}$ results in $Cu_{47.5}Zr_{47.5}Al_5$, a bulk-forming alloy whose properties are well documented [1,2,10,11,23–26]; $Cu_{47.5}Zr_{47.5}Al_5$ exhibits significantly higher plasticity and GFA than $Cu_{50}Zr_{50}$. The addition of Al to $Cu_{50}Zr_{50}$ also increases in its yield strength (σ_y), Young's modulus (E) and onset glass transition temperature (T_g), as summarized in Table 1. Given these observations, $Cu_{47.5}Zr_{47.5}Al_5$ is an excellent choice for evaluating the effects of the addition of a minor element on the development of glassy structures that are responsible for the simultaneous improvements in these competing properties, i.e. plasticity and GFA. In addition, to ensure the validity of the analyses, two alloys, $Cu_{50}Zr_{50}$ and $Cu_{65}Zr_{35}$, which were documented in an earlier study [14], were reanalyzed.

Table 1
Selected thermomechanical properties of $Cu_{65}Zr_{35}$, $Cu_{50}Zr_{50}$ and $Cu_{47.5}Zr_{47.5}Al_5$, measured using 1 mm diameter rods of the alloys.

Alloy	GFA (mm)	ε_p (%)	σ_y (MPa)	E (GPa)	T_g (°C)
$Cu_{50}Zr_{50}$	1–2	5	1740	82.5	404
$Cu_{47.5}Zr_{47.5}Al_5$	3	11	1790	87.3	420
$Cu_{65}Zr_{35}$	2	0	2230	115.5	463

Note: Both ε_p and σ_y were measured by compression tests [6], while E was measured by the nanoindentation technique [6]. The values are averages of 10 measurements recorded per specimen.

3. MD simulations and structural analyses

Two computational amorphous alloys, $Cu_{50}Zr_{50}$ and $Cu_{47.5}Zr_{47.5}Al_5$, with distinctly different mechanical properties, were synthesized using classical MD simulations via techniques used in previously reported experimental and simulation studies of the structure–property relationship of alloys [4,6,12]. The embedded atom method (EAM) potential describing the interatomic interactions in the Cu–Zr–Al ternary system [9] was employed to prepare the glassy $Cu_{50}Zr_{50}$ and $Cu_{47.5}Zr_{47.5}Al_5$ samples. Approximately 32,000 atoms corresponding to the stoichiometric compositions of $Cu_{50}Zr_{50}$ and $Cu_{47.5}Zr_{47.5}Al_5$ were first packed into a simulation cell with the approximate dimensions of $10.2 \times 8.3 \times 6.7$ nm and then heated to a temperature (2,100 K) that is above the melting points of both alloys. Next, before being quenched, the two samples were allowed to relax for 10 ns (time step = 1 fs) at 2,100 K to obtain randomly mixed liquids. Note that this treatment ensures the glassy structures of the quenched samples are independent of the initial atomic configurations. The randomly mixed samples were then quenched to 300 K at the rate of 5×10^{11} K s^{-1} to produce the 3-D amorphous solids. A fixed number of particles, pressure and temperature (i.e. an NPT ensemble) were used for the quenching process, with the temperature controlled by a Nosé–Hoover thermostat [27] and the pressure controlled at zero using a Nosé–Hoover barostat [28].

A periodic boundary condition (PBC) was applied to all three directions in order to eliminate any surface effects. The model alloys with the PBC were deformed at 300 K by applying a simple shear strain at a rate of 10^8 s^{-1} to induce structural disordering. The atomic-scale structures of the quenched alloys and their evolution during the simple shear deformation were analyzed in terms of the SROs identified using the weighted Voronoi tessellation technique (hereinafter, Voronoi analysis) [4]. Further analyses were performed to examine the connections between neighboring SROs in constructing MROs. The other specifications of the MD simulations and analysis techniques used in this study are described in detail elsewhere [4,29].

4. Results and discussion

4.1. Local structures of the alloys in terms of SROs

Although the potential used for the MD simulations has already been extensively validated against a large set of experimentally measured properties and *ab initio* data [30], the reliability of the potential was tested again by determining the nearest average interatomic distances (i.e. bond lengths) of the atomic pairs comprising the model alloys. The bond lengths of the atomic pairs were determined by calculating the partial radial distribution functions (RDFs) of $Cu_{50}Zr_{50}$ and $Cu_{47.5}Zr_{47.5}Al_5$ as shown in Fig. 1. The present calculations agreed reasonably well with the results of the experimental measurements performed using high-energy X-ray diffractometry [31–35] and those of simulations based on other reported empirical potentials [35–38], as well as those obtained by adding the tabulated radii of the atomic species [39]. This was evidence that the EAM potential used in this study was suitable for describing the local structures of the actual amorphous alloys. It should be noted that the calculated bond length between Al and Cu was markedly shorter than the algebraic sum of the tabulated radii of the same species. This was attributed to the electronic interaction between Al and Cu atoms [30] and could be the basis for stable icosahedral packing in the presence of Al atoms as will be discussed later.

We first calculated the mechanical responses of the model alloys, since they are directly related to the experimentally measured properties of the alloys. Fig. 2 shows the stress–strain curves of the model alloys calculated by applying simple shear strain (γ). Of the two alloys, $Cu_{47.5}Zr_{47.5}Al_5$ exhibited a slightly higher yield strength and shear modulus; this result was consistent with that of the experiments (Table 1). The plasticity of the alloys could also be determined from the stress–strain curves in Fig. 2. Considering that the dimensions of the samples used in this study were smaller than the typical thickness (10–20 nm) of a shear band, the stress–strain curves of the model alloys in Fig. 2 can be regarded as being representative of the characteristic flows of the materials within their respective shear bands: both alloys exhibited an abrupt decrease in strength after reaching the critical strength (τ_y) at $\gamma \approx 0.1$, beyond which their strengths plateaued at a steady-state value (τ_s). Here, τ_y and τ_s can be regarded as the global yield strength of the undeformed amorphous solid and the strength of the material inside a propagating shear band, respectively [7]. The normalized difference ($\Delta\tau/\tau_y$) between these stresses, therefore, corresponds to the extent of structural softening, which determines the tendency towards strain localization. It was hence used as a parameter to evaluate the plasticity of the amorphous alloys [7,14]. Although the values of $\Delta\tau/\tau_y$ did not seem to change significantly with the structures of the alloys, $Cu_{47.5}Zr_{47.5}Al_5$ exhibited a comparatively smaller $\Delta\tau/\tau_y$ value, indicating that $Cu_{47.5}Zr_{47.5}Al_5$ has a lower tendency to undergo strain localization. Since the degree of strain localization, i.e. plasticity, is structure dependent, the different degrees of strain localization observed from the model alloys was

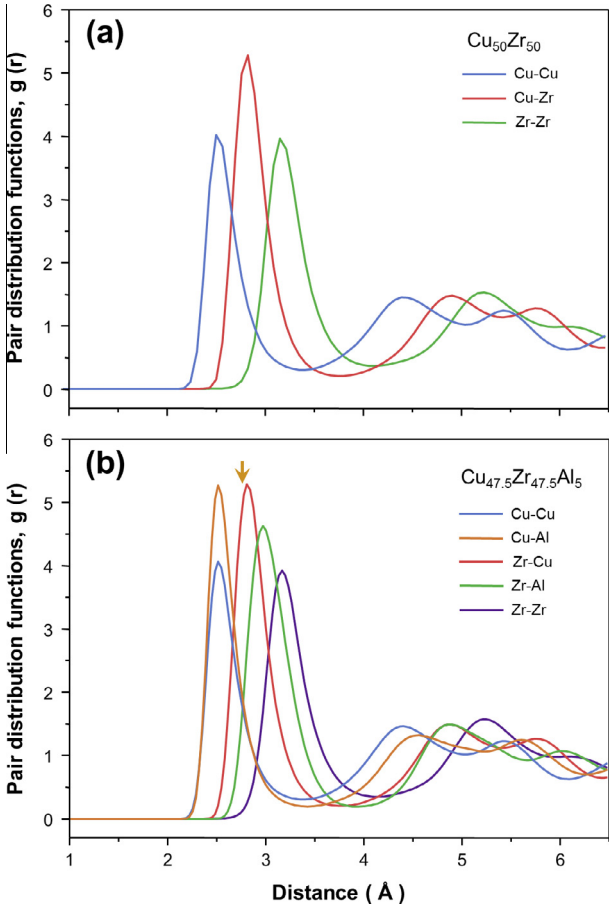

Fig. 1. Partial RDFs calculated from the simulated (a) $Cu_{50}Zr_{50}$ and (b) $Cu_{47.5}Zr_{47.5}Al_5$ alloys (insets). The arrow in (b) denotes the bond length of the Al–Cu pair obtained on the basis of the algebraic sum of the atomic radii of the same species, indicating the occurrence of bond shortening between Cu–Al pairs in the amorphous alloy $Cu_{47.5}Zr_{47.5}Al_5$.

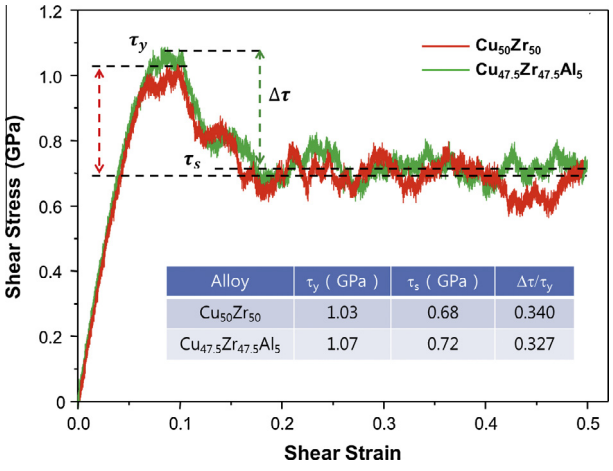

Fig. 2. Simulated stress–strain curves of the $Cu_{50}Zr_{50}$ and $Cu_{47.5}Zr_{47.5}Al_5$ amorphous solids, calculated by applying simple shear strain.

accounted for by resolving the initial atomic-scale structures and their transformation during deformation.

Before the glassy structures of $Cu_{50}Zr_{50}$ and $Cu_{47.5}Zr_{47.5}Al_5$ could be described in terms of MROs, the local structures of the alloys were resolved in terms of SROs using the Voronoi tessellation method. Fig. 3a shows the fractions of the polyhedra in $Cu_{50}Zr_{50}$ and $Cu_{47.5}Zr_{47.5}Al_5$ with central Cu, Zr, and Al atoms, calculated for different coordination numbers (CNs). The centers of the polyhedra with $11 \leqslant CN \leqslant 13$ were occupied mostly by the smaller atoms, i.e. either Cu or Al, while the larger atom, Zr, was the most common atom occupying the centers of the less stable polyhedra with CNs significantly greater than 12. When accounting for all polyhedra with $11 \leqslant CN \leqslant 13$, their fractions were 44.7% and 46.4% for $Cu_{50}Zr_{50}$ and $Cu_{47.5}Zr_{47.5}Al_5$, respectively, indicating that $Cu_{47.5}Zr_{47.5}Al_5$ has a comparatively more ordered structure.

When accounting for the icosahedral orders with $CN = 12$, the effect of the minor alloying with Al on the formation of a well-ordered structure was more pronounced. Fig. 3b shows the populations of the most dominant/populous types of icosahedral orders with $CN = 12$.

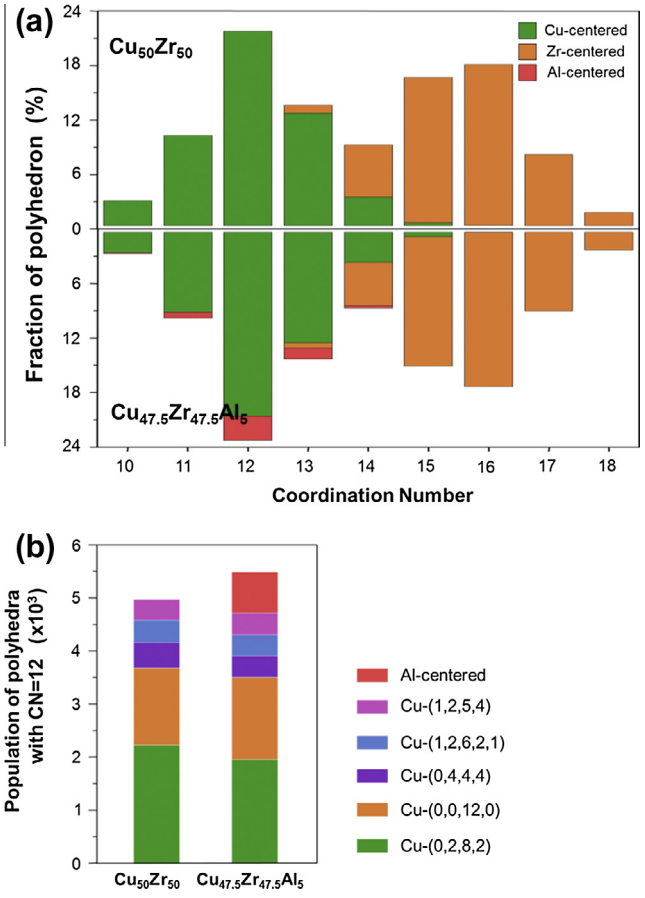

Fig. 3. (a) Fractions of the various polyhedra in $Cu_{50}Zr_{50}$ and $Cu_{47.5}Zr_{47.5}Al_5$ with Cu, Zr and Al atoms at the center, calculated for different CNs. (b) Fractions of the most populous types of icosahedra with $CN = 12$ in $Cu_{50}Zr_{50}$ and $Cu_{47.5}Zr_{47.5}Al_5$. It is clear that the additional icosahedral orders are due to Al.

There were ~10% more icosahedral orders ($CN = 12$) in $Cu_{47.5}Zr_{47.5}Al_5$ than in $Cu_{50}Zr_{50}$ (there were 5490 icosahedral orders in $Cu_{47.5}Zr_{47.5}Al_5$ and 4974 in $Cu_{50}Zr_{50}$). When analyzing the types of icosahedral orders in $Cu_{47.5}Zr_{47.5}Al_5$ on the basis of the atoms at their centers, 86% of all the icosahedral orders were found to have Cu at the center, while 14% were Al centered. Considering that the alloy contains only 5% Al, this result indicates the ability of Al to form additional icosahedral orders in $Cu_{47.5}Zr_{47.5}Al_5$. In particular, when analyzing the central atoms of the "full" icosahedra, denoted by a Voronoi index of $(0,0,12,0)$, in $Cu_{47.5}Zr_{47.5}Al_5$, 16.3% of all the Al atoms added to the alloy occupied the centers of full icosahedra, while only 10.2% of all the Cu atoms were at the centers. The above analyses derived on the basis of the results shown in Fig. 3b provide clear evidence that the alloying of Al facilitated the formation of additional icosahedra, with Al being preferentially present at their centers. That the fraction of the icosahedral orders in $Cu_{47.5}Zr_{47.5}Al_5$ was larger makes this alloy more ordered and stable.[2] These characteristics, in turn, result in the GFA, strength, modulus and T_g of the alloy being greater than those of $Cu_{50}Zr_{50}$. However, this analysis, which is based on the SROs in $Cu_{47.5}Zr_{47.5}Al_5$, is unable to explain its high plasticity. Therefore, an explanation based on another structural hierarchy is necessary.

4.2. Local structures of the alloys in terms of icosahedral MROs or ICOI

There are two important points to consider when describing the relationship between the properties of bulk amorphous alloys and their structures: (i) the properties of the alloys are closely related to their packing density [5,6,40]; and (ii) the packing density of the alloys is determined by the degree of SRO [4–7]. In view of these observations, the plasticity and GFA of an alloy are contrasting properties and exhibit inverse proportionality, which stems from the fact that the properties have different structural bases. Therefore, the observation that the number of icosahedral orders in $Cu_{47.5}Zr_{47.5}Al_5$ was greater, resulting in the GFA and strength of the alloy also being higher, at first seems a contradiction when it comes to explaining the fact that the plasticity of this alloy was also higher. However, this seeming contradiction can be explained by elucidating the different effects the icosahedra have on the kinetic and dynamic behaviors of the alloy during cooling and deformation, respectively.

In terms of kinetics, the icosahedra are short-range structures that retard crystallization during cooling and thus contribute to the improvement in the GFA. Thus,

[2] Even though the alloy composition used in this study was slightly different from that used in a previous study ($Cu_{46}Zr_{47}Al_7$) [9], the conclusion arrived at here is similar to that obtained in the previous one, namely that the minor alloying of $Cu_{46}Zr_{54}$ with Al facilitated the formation of icosahedra.

$Cu_{47.5}Zr_{47.5}Al_5$, which has a lager fraction of icosahedral ordering, exhibits a higher GFA; this issue has been analyzed extensively in many earlier studies [6,13,41–43]. On the other hand, from a dynamics viewpoint, the icosahedra are the major structural motif, which, upon deformation, undergo preferential disordering/shear transformation [6]. Therefore, they are the major source for new flow defects, which are required to sustain the plastic flow at a given rate. The tendency for structural disordering exhibited by each icosahedron is different and depends on the species of its central atom and the atomic configuration of the first coordination shell of the icosahedron. This is because these two characteristics are the major parameters determining the mechanical stability of the individual icosahedra and the associated medium-range structures, and result in the icosahedra exhibiting different resistances to structural disordering. This point will be addressed here in detail by clarifying the role of Al in the development of the unique shell structures of the icosahedra and their medium-range structures during cooling, as well as the subsequent disordering behaviors of the icosahedra during deformation.

In a previous study, we had shown that individual icosahedra in Cu–Zr binary alloys can connect to neighboring ones to form various types of icosahedral MROs [14]. Different icosahedral MROs, owing to differences in the bonding force (or potential energy), exhibit different structural stabilities [14,44,45], and, as a result, different disordering behaviors [14]. It is therefore necessary to consider how the icosahedra in $Cu_{47.5}Zr_{47.5}Al_5$ are connected to one another over the medium range before one can more realistically describe the local glassy structure of the ternary alloy and relate it to the disordering behavior of the icosahedra. We do so by first examining how the individual icosahedra form MROs. Of the various icosahedral MROs present in the alloys [14,46], the "volume-sharing" type (also referred to as the "interpenetrating", "pentagonal bicap-sharing", "cap-sharing" or "tetrahedral-sharing" type, depending on the author) is not only statistically dominant, but also exhibits the lowest potential energy [14], the smallest atomic volume [14,44] and, possibly, the highest stiffness [44]. This particular type of MRO is produced when some of the surrounding atoms in the first coordination shell of an icosahedron are also the centers of its neighboring icosahedra. This type of linking with neighboring icosahedra results in volume-sharing icosahedra that share five common neighboring atoms. These types of structures are medium range in nature, and constitute ICOIs, as shown in Fig. 4a [14]. During the formation of an ICOI, each icosahedron can also share its volume with different numbers of neighboring icosahedra as shown in Fig. 4a–d. This number is referred to as the bond number (N) (i.e. the number of atoms in the first coordination shell that are also the centers of other icosahedra) and is used in this study as a parameter for quantifying either the degree of the ICOIs themselves or the degree of the MROs of the amorphous alloys.

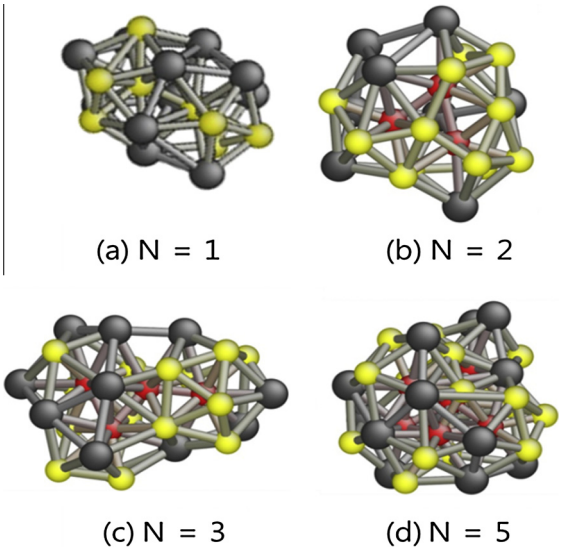

Fig. 4. Representative configurations of ICOIs with different bond numbers (N) present in the simulated alloy $Cu_{50}Zr_{50}$: (a) $N = 1$, (b) $N = 2$, (c) $N = 3$ and (d) $N = 5$. The yellow (small) and grey (large) spheres represent Cu and Zr atoms, respectively, while the red spheres represent Cu atoms centered in the individual icosahedra. (For interpretation of the references to colour in this figure legend, the reader is referred to the web version of this article.)

As was the case with the SROs [4–6,41,42,47], the fractions of the MROs were also composition sensitive. The total numbers of full icosahedra with a Voronoi index of $(0,0,12,0)$ were found to be 1474 (4.5%) and 1811 (5.7%) for $Cu_{50}Zr_{50}$ and $Cu_{47.5}Zr_{47.5}Al_5$, respectively. These icosahedra combined with their neighboring icosahedra to form ICOIs with different degrees of MRO. Fig. 5a shows the populations of the various ICOIs with different N values for $Cu_{50}Zr_{50}$ and $Cu_{47.5}Zr_{47.5}Al_5$. In both alloys, the population of the icosahedra varied similarly as a function of N. However, compared with the icosahedra in $Cu_{50}Zr_{50}$, those in $Cu_{47.5}Zr_{47.5}Al_5$ were more likely to combine with their neighboring icosahedra and, thus, had a slightly higher tendency to form medium-range structures. We quantified the degrees of MRO of the two alloys in terms of the average bond number ($\bar{N}$) of the ICOIs and found the degrees to be 1.96 and 2.18 for $Cu_{50}Zr_{50}$ and $Cu_{47.5}Zr_{47.5}Al_5$, respectively. This suggests that $Cu_{47.5}Zr_{47.5}Al_5$ is more ordered and stable even when it is evaluated from the MRO point of view; this was further support of the fact that $Cu_{47.5}Zr_{47.5}Al_5$ exhibits a higher GFA, strength, modulus and T_g than does $Cu_{50}Zr_{50}$.

The two different medium-range structures of the model alloys in Fig. 5a must be related to the minor element (Al) added to $Cu_{50}Zr_{50}$. Therefore, we examined the role played by Al in the formation of the various ICOIs by classifying all icosahedra in $Cu_{47.5}Zr_{47.5}Al_5$ according to the species of their central atoms. Fig. 5b shows the relative fractions of the Cu- and Al-centered icosahedra (hereafter, denoted as Cu- and Al-$(0,0,12,0)$) calculated for each group of ICOIs with different N values in $Cu_{47.5}Zr_{47.5}Al_5$. With an increase in the N value of the ICOIs in $Cu_{47.5}Zr_{47.5}Al_5$, the fraction of Cu-$(0,0,12,0)$ in each ICOI group increased,

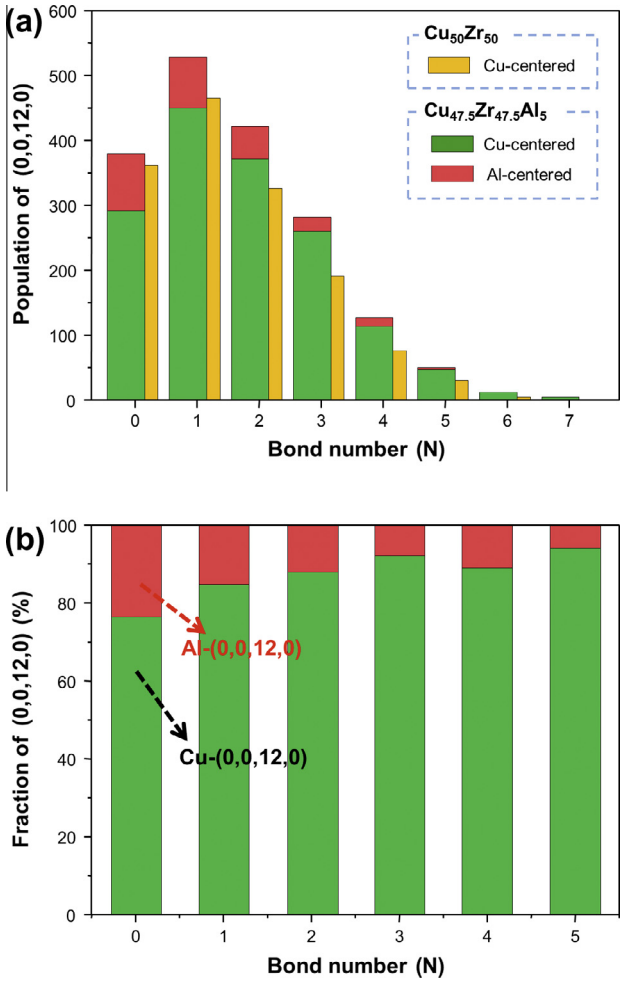

Fig. 5. (a) Variations in the populations of the icosahedra with different N values in $Cu_{50}Zr_{50}$ and $Cu_{47.5}Zr_{47.5}Al_5$. Note that the species of the central atoms of the icosahedra in $Cu_{47.5}Zr_{47.5}Al_5$ is either Cu or Al, resulting in Cu- and Al-centered icosahedra, respectively. (b) Changes in the relative fractions of the Cu- and Al-centered icosahedra (denoted as Cu- and Al-(0, 0, 12, 0), respectively) for each group of ICOIs with different N values in $Cu_{47.5}Zr_{47.5}Al_5$, as evaluated from (a).

while that of Al-(0, 0, 12, 0) decreased. This analysis indicates that, compared to Cu-(0, 0, 12, 0), Al-(0, 0, 12, 0) had a lower tendency to cluster and form MROs. We quantified the clustering tendencies of these two different types of icosahedra in terms of the average N value ($\bar{N}$) of the ICOIs and found them to be 2.04 and 1.69 for Cu- and Al-(0, 0, 12, 0), respectively. Combining the results in Fig. 5a and b, it is clear that the addition of Al to $Cu_{50}Zr_{50}$ increased the total population of (0, 0, 12, 0) by facilitating the formation of extra Al-(0, 0, 12, 0). However, these Al-(0, 0, 12, 0), in contrast to Cu-(0, 0, 12, 0), did not readily form high-degree medium-range structures as determined by the N values of the ICOIs.

4.3. Role of Al in the formation of icosahedral MROs

The question that arises next is why is it that Cu-(0, 0, 12, 0) and Al-(0, 0, 12, 0) have different tendencies to form ICOIs. Considering that the smaller atoms, i.e. those of Cu and Al, in the first coordination shell of an icosahedron can also be the central atoms of the neighboring icosahedra, the observed differences in the clustering tendencies of Cu-(0, 0, 12, 0) and Al-(0, 0, 12, 0) can be attributed to the different configurations of the shell structures of the icosahedra. We determined the atomic ratios of Zr:Cu:Al in the first coordination shell of Cu-(0, 0, 12, 0) and Al-(0, 0, 12, 0) and found them to be on average 6.3Zr:5.2Cu:0.5Al and 7.3Zr:4.6Cu:0.1Al, respectively. Therefore, when compared to the first shell of Cu-(0, 0, 12, 0), that of Al-(0, 0, 12, 0) was richer in Zr, but leaner in Cu and Al. In particular, Al-(0, 0, 12, 0) with $N = 0$ and 1, which accounted for the majority (71.4%) of all Al-(0, 0, 12, 0), possessed only 4.3 Cu atoms in the first coordination shell; this value is considerably smaller than the average number of Cu atoms (=5.2) in the first coordination shell of Cu-(0, 0, 12, 0). Thus, the question arises: why are the coordination shells of Al-(0, 0, 12, 0) lean in Cu and how do these Cu-lean shell structures of Al-(0, 0, 12, 0) lower the clustering tendency and, consequently, the structural stability of Al-(0, 0, 12, 0)? The answers to these questions may explain why Al-(0, 0, 12, 0) does not readily form ICOIs with high N values. However, before these fundamental questions can be answered, it is necessary to review the topology, electronic interaction and chemistry of the constituent elements of the alloys in question as has been done in Ref. [9], and relate these characteristics to stable icosahedral packing of Al-(0, 0, 12, 0) and its formation of ICOIs.

When viewed from a topological perspective, the atomic size ratio Al:Zr (=0.905) is much closer to the value (0.902) required for ideal icosahedral packing [48] than those of Cu:Zr (=0.810) and Zr:Zr (=1.000). This implies that an icosahedron would be topologically more stable when Al occupies the center and the coordination shell consists of Zr atoms only. However, considering that the alloy composition considered in this study is abundant in Cu (47.5%), the formation of Al-(0, 0, 12, 0) with Zr-only coordination shell is statistically infeasible. Instead, the formation of Al-(0, 0, 12, 0) with mixed atomic species in the shell is more likely because of the electronic interaction and chemistry between the constituent elements of the system. First, the formation of stable Al-(0, 0, 12, 0) can be explained on the basis of the bond shortening between Al and Cu [9]. As shown in Fig. 1, as well as by previous simulations [9] and experimental measurements [49], the actual interatomic spacing between Al and Cu is smaller than the algebraic sum of the tabulated radii of Al and Cu. This bond shortening between Al and Cu allows Cu to effectively occupy the space of the coordination shell of Al-(0, 0, 12, 0), in a manner similar to how Zr does so. In other words, when Al–Cu bond shortening occurs (position D in Fig. 6), the angle measured from the central Al atom to a neighboring Cu atom is similar to that made by a Zr atom (position E in Fig. 6), allowing Cu atoms to be in full contact with the neighboring Zr atoms. Therefore, even with

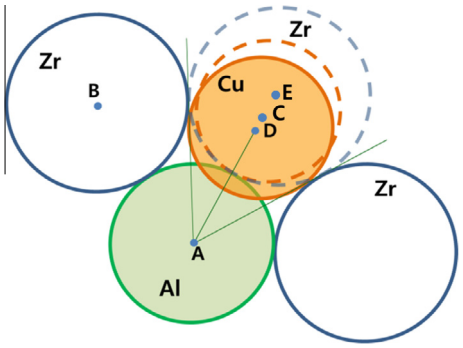

Fig. 6. Schematic of the bond shortening between Al–Cu pairs, which results in close packing and leads to the formation of Al-(0,0,12,0). In the absence of the shortening of the Al–Cu bond, the position C would be occupied by Cu (the center of the dashed orange circle). This would leave an empty space between the atoms in the coordination shell. However, because of the shortening of the bond between the Al–Cu pair, Cu is actually found at D and the empty space is eliminated. The position E is the center of the dashed blue circle, representing Zr. ([Reproduction of Fig. 4 in Ref. [9]].) (For interpretation of the references to colour in this figure legend, the reader is referred to the web version of this article.)

the presence of a significant fraction of Cu atoms in the coordination shell of Al-(0,0,12,0), Al-(0,0,12,0) can still be densely packed and, thus, be topologically stable. Second, the calculated mixing enthalpies between any two species in the ternary system, e.g. Al–Cu and Al–Zr pairs, are all negative. This provides the basis as to why the central Al atoms of (0,0,12,0) in $Cu_{47.5}Zr_{47.5}Al_5$ can be surrounded by both Zr and Cu atoms. However, since the mixing enthalpy between Al–Zr pairs ($-43.4\ kJ\ mol^{-1}$) is even lower than that of Al–Cu pairs ($-23.2\ kJ\ mol^{-1}$) [30], the central Al atom of an icosahedron tends to bind with more Zr atoms [9]. This characteristic of Al atoms promotes the formation of stable Al-(0,0,12,0) with a Zr-rich (or inversely, Cu-lean) coordination shell. This, in turn, causes Al-(0,0,12,0) to form a lower-degree medium-range structure as discussed below.

It is emphasized that, in order for an icosahedron to form ICOIs with high N values, the first shell of the icosahedron should be rich in Cu (and Al). This is because the Cu (and Al) atoms in the first shell can also act as the centers of the neighboring icosahedra, forming ICOIs. By this argument, Al-(0,0,12,0), owing to its Cu-lean (also Al-lean) coordination shell, is unable to form ICOIs with high N values. We quantified the tendencies of the various icosahedra to form medium-range structures in $Cu_{47.5}Zr_{47.5}Al_5$ and found the $\bar{N}$ value of Al-(0,0,12,0) to be 1.69, while that of Cu-(0,0,12,0) was 2.04. This low clustering tendency of Al-(0,0,12,0), which is attributable to its Cu-lean coordination shell, would affect the structural stability of Al-(0,0,12,0) and, thus, their disordering behaviors during deformation.

4.4. Shear transformation behaviors of ICOIs

In a previous study, we have shown that, when the degree of ICOIs in a binary alloy is high, it restrains the atomic mobility (see Fig. 9b in Ref. [14]); this, in turn, hinders the formation of new flow defects associated with deformation. This suggests a possible correlation between the medium-range structures and plasticity in ternary alloys. Considering that $Cu_{50}Zr_{50}$ and $Cu_{47.5}Zr_{47.5}Al_5$ have different medium-range structures as quantified by the different fractions of ICOIs with different N values, these two alloys would experience different degrees of structural disordering under an imposed stress. We first evaluated the structural stabilities of the various ICOIs comprising the model alloys. Fig. 7 shows the variations in the fractions of the disrupted icosahedra evaluated according to the N values and species of the central atoms of the icosahedra in $Cu_{50}Zr_{50}$ and $Cu_{47.5}Zr_{47.5}Al_5$ that were subjected to homogeneous deformation ($\gamma = 0.05$). Of the various types of icosahedra, Al-(0,0,12,0) appeared to be slightly more susceptible to shear transformation. In general, however, the structural stabilities of the icosahedra in both alloys were more sensitive to the N value than to the species of the central atoms of the icosahedra: the icosahedra that bonded to fewer neighboring icosahedra (i.e. ICOIs with a smaller N) were more prone to disruption, whereas those with a larger N displayed comparatively less disruption.

In order to determine which types of icosahedra are more susceptible to disordering and contribute to the creation of flow defects, we analyzed the results in Fig. 7 in terms of the variations in the populations of the disrupted icosahedra in $Cu_{50}Zr_{50}$ and $Cu_{47.5}Zr_{47.5}Al_5$ as functions of the N values and the species of the central atoms of the icosahedra. Fig. 8 shows the variations in the population of the disrupted icosahedra in $Cu_{50}Zr_{50}$ and $Cu_{47.5}Zr_{47.5}Al_5$ with respect to N and the species of the central atoms, when subjected to a homogeneous deformation ($\gamma = 0.05$). The total numbers of the disrupted icosahedra were 540 and 656 for $Cu_{50}Zr_{50}$ and $Cu_{47.5}Zr_{47.5}Al_5$, respectively, indicating that $Cu_{47.5}Zr_{47.5}Al_5$ underwent far more extensive disordering (23% greater) than $Cu_{50}Zr_{50}$. When classifying

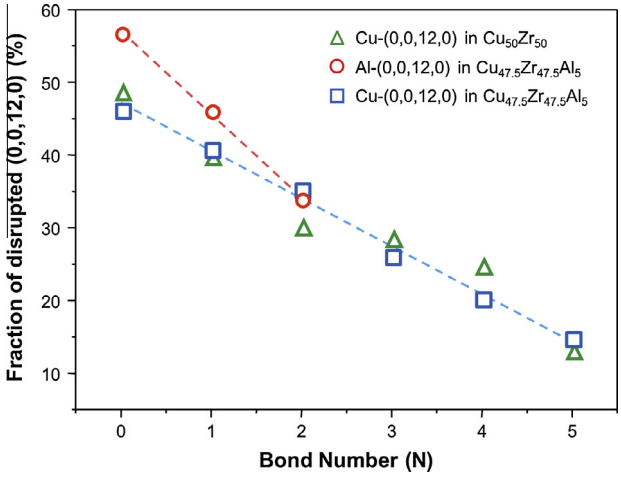

Fig. 7. Variations in the fractions of the icosahedra in $Cu_{50}Zr_{50}$ and $Cu_{47.5}Zr_{47.5}Al_5$ that were disrupted during homogeneous deformation ($\gamma = 0.05$) as a function of N.

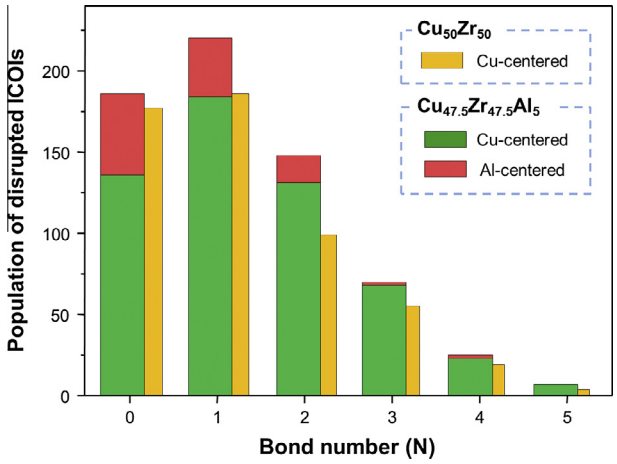

Fig. 8. Variations in the population of the disrupted icosahedra/ICOIs counted as a function of the N values and the species of the central atoms in $Cu_{50}Zr_{50}$ and $Cu_{47.5}Zr_{47.5}Al_5$ subjected to homogeneous deformation ($\gamma = 0.05$).

the disrupted icosahedra in both alloys on the basis of the N values, it was found that nearly 85% of the disruptions took place in the icosahedra with $N \leqslant 2$. Further, when the species of the central atoms was considered, 82% and 95% of the icosahedra with $N \leqslant 2$ were destroyed in Cu-$(0,0,12,0)$ and Al-$(0,0,12,0)$,[3] respectively, indicating that Al-$(0,0,12,0)$ was more susceptible to disruption. Overall, $Cu_{47.5}Zr_{47.5}Al_5$, even with its higher-degree medium-range order as determined by the $\overline{N}$ values of its ICOIs, underwent more prominent structural disordering owing to the breakdown of Al-$(0,0,12,0)$, which tended to form comparatively lower-degree ICOIs.

As discussed earlier, the icosahedra or ICOIs with small N values preferentially underwent disruption under imposed stress. The disrupted icosahedral sites correspond to regions that have comparatively loose packing and, thus, can be feasible sites where local deformations nucleate. This breakdown of icosahedra, on the one hand, is necessary to bear the externally applied strain. On the other hand, it causes structural softening and hence can lead to strain localization. This suggests that even if intense disordering is necessary for accommodating an externally applied strain, it may not be the only factor that determines the degree of plasticity. Recent MD simulations, which studied the effect of the composition [4–7] and cooling rate [3] of amorphous alloys on their strain localization behaviors, showed that (embryonic) shear bands formed at locations at which disordering was intense. This suggests that the degree of localization is strongly dependent on the spatial distribution of the disrupted icosahedra. Therefore, any discussion of the degree of strain localization in amorphous alloys should take into account the spatial distribution of the disrupted icosahedra as well as their population. Shi

[3] The fractions of disrupted icosahedra were calculated by dividing the numbers of disrupted icosahedra with $N \leqslant 2$ by the total number of disrupted icosahedra.

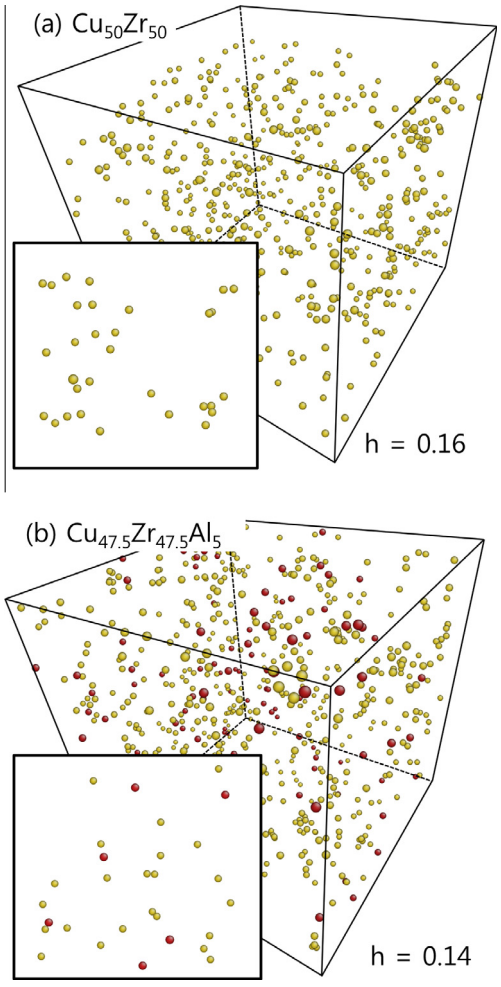

Fig. 9. Snapshots showing the spatial distribution of the disrupted icosahedral sites in (a) $Cu_{50}Zr_{50}$ and (b) $Cu_{47.5}Zr_{47.5}Al_5$ when subjected to $\gamma = 0.05$. In these figures, only the central atoms of the disrupted icosahedra are plotted as points in the simulation box. The different colors indicate the different types of icosahedra: yellow, disrupted Cu-$(0,0,12,0)$; red, Al-$(0,0,12,0)$). In order to be able to visualize better the location of the disrupted icosahedra, only the icosahedra within a slab with a thickness of ~1 nm are shown in the insets. (For interpretation of the references to colour in this figure legend, the reader is referred to the web version of this article.)

and Falk [3,8] have assessed the effects of the spatial distribution and percolation of SROs on the mechanical response of amorphous alloys. However, for this issue, much remains to be uncovered and analyzed in detail.

Before analyzing the effect of the spatial distributions of the disrupted icosahedra on the global plasticity of the present alloys, we reanalyzed two computational alloys, $Cu_{50}Zr_{50}$ and $Cu_{65}Zr_{35}$, which have been documented previously elsewhere [14]. $Cu_{50}Zr_{50}$ and $Cu_{65}Zr_{35}$ exhibited a pronounced difference in their initial atomic-scale structures and thus underwent distinctly different structural evolutions [29]. In comparison to that of $Cu_{50}Zr_{50}$, $Cu_{65}Zr_{35}$ has a more ordered structure with a higher packing density. When loaded at stresses below its global yield strength, $Cu_{65}Zr_{35}$ exhibits more intense structural disordering as demonstrated by the results of simulations [5,14,29] and

experiments [5,29,50]. A previous study of the relation between structural disordering and strain localization [4,51–55] had found that the intense disordering observed in $Cu_{65}Zr_{35}$ caused more pronounced strain localization, making it infeasible for the alloy to mediate large plastic strains; this was also confirmed by experiments.

The interpretation mentioned above, which only considered the degree of disordering, however, is unable to explain why the plasticity of $Cu_{47.5}Zr_{47.5}Al_5$ is greater, when it also undergoes intense structural disordering to an extent similar to that experienced by $Cu_{65}Zr_{35}$. Before explaining the role of the spatial distribution of the disrupted icosahedra in $Cu_{47.5}Zr_{47.5}Al_5$, we reanalyze why $Cu_{65}Zr_{35}$ exhibited more intense strain localization, by taking into account the spatial distributions of its disrupted icosahedra. In order to assess the effect of the spatial distributions of the disrupted icosahedra on strain localization, we defined a structural parameter (h) that can be used to quantify the spatial distribution (or uniformity) of the disrupted icosahedra in the 3-D spaces of the computational alloys $Cu_{50}Zr_{50}$ and $Cu_{65}Zr_{35}$. (The detailed procedures for deriving the mathematical equation that can quantify the spatial distribution (h) of the disrupted icosahedra is provided in the **Appendix A**.) The h values of the disrupted icosahedra in $Cu_{65}Zr_{35}$ and $Cu_{50}Zr_{50}$ when subjected to a deformation ($\gamma = 0.05$) were 0.17 and 0.15, respectively. The higher h value exhibited by the deformed $Cu_{65}Zr_{35}$ indicates that, in comparison to the distribution of the disrupted icosahedra in $Cu_{50}Zr_{50}$, their distribution in $Cu_{65}Zr_{35}$ was less uniform; this is shown schematically in Fig. A1 in the **Appendix A**. Therefore, even though the population of the disrupted icosahedra within $Cu_{65}Zr_{35}$ was greater, their non-uniform distribution is likely to cause more intense strain localization, resulting in lower plasticity.

We now turn our attention to the model alloys considered in this study, $Cu_{50}Zr_{50}$ and $Cu_{47.5}Zr_{47.5}Al_5$. Fig. 9 shows snapshots of the distributions of the disrupted icosahedra within $Cu_{50}Zr_{50}$ and $Cu_{47.5}Zr_{47.5}Al_5$ when subjected to a homogeneous shear deformation ($\gamma = 0.05$). When quantifying the spatial distribution of the disrupted icosahedra in the model alloys (Fig. 10), the h value decreased with an increase in the strain, indicating that the uniformity of the spatial distributions increased with the strain. Of the two alloys, however, the h values were comparatively smaller for $Cu_{47.5}Zr_{47.5}Al_5$ for all strains. These results indicate that even when a large number of disrupted icosahedra were present in the model alloys, they tended to distribute more evenly in $Cu_{47.5}Zr_{47.5}Al_5$. This probably reduced strain localization through the spreading of the shear transformation over the entire volume of the alloy.

In summary, the addition of 5% Al to $Cu_{50}Zr_{50}$ promoted the formation of additional Al-(0, 0, 12, 0), making the alloy more ordered. These additional Al-(0, 0, 12, 0), owing to their Cu-lean shell structures, are unable to form ICOIs with high N values and, thus, are structurally less stable. As a result, they undergo more pronounced disruption during deformation. Even though the population of the disrupted icosahedra in $Cu_{47.5}Zr_{47.5}Al_5$ was larger, their spatial distribution as evaluated by h was more uniform than that in $Cu_{50}Zr_{50}$. Overall, in comparison to $Cu_{50}Zr_{50}$, $Cu_{47.5}Zr_{47.5}Al_5$ is more ordered when it comes to both SROs and MROs, and therefore exhibits higher strength, GFA and T_g. During deformation, more fertile sites for local deformation are produced in $Cu_{47.5}Zr_{47.5}Al_5$ through the spreading of the shear transformation of the ICOIs with lower N values. This reduces strain localization in $Cu_{47.5}Zr_{47.5}Al_5$ and allows it to accommodate larger strains. This quantitative analysis provides insight into the underlying physics of why an alloy with a more ordered structure can exhibit less intense shear localization during deformation.

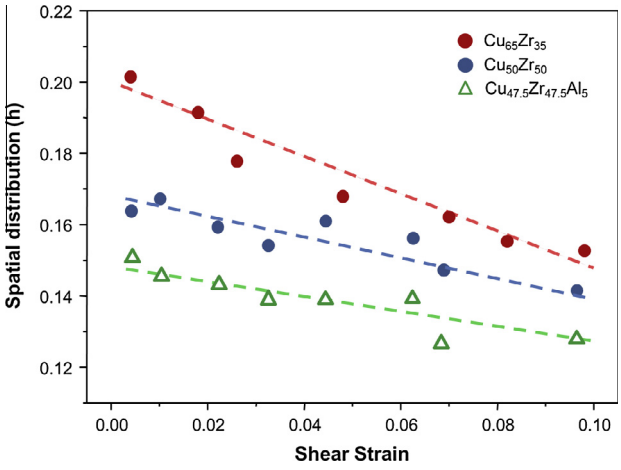

Fig. 10. Variations in the spatial distributions of the disrupted icosahedra calculated as a function of the strain imposed on $Cu_{65}Zr_{35}$, $Cu_{50}Zr_{50}$ and $Cu_{47.5}Zr_{47.5}Al_5$.

5. Conclusion

In this study, the glassy structures of $Cu_{50}Zr_{50}$ and $Cu_{47.5}Zr_{47.5}Al_5$ were resolved in terms of SROs and MROs to explore their effect on the thermomechanical properties of the alloys. It was found that, in both alloys, the structural stabilities of the icosahedra depend largely on their bond numbers such that an icosahedron becomes mechanically more stable by forming ICOIs with a greater number of neighboring icosahedra. This causes it to become less susceptible to disordering during shear deformation. This approach of taking into consideration the medium-range structures of the alloys goes beyond previous analyses of the structure–property relationship, which had only considered the SROs and produced self-consistent results even in a ternary alloy that exhibited seemingly contradictory properties.

The addition of Al to $Cu_{50}Zr_{50}$ increases the total population of (0, 0, 12, 0) by facilitating the formation of additional Al-(0, 0, 12, 0); these cause $Cu_{47.5}Zr_{47.5}Al_5$ to have higher-degree medium-range structures, as determined by the high $\overline{N}$ value, such that the icosahedra are more exten-

sively connected to one another in an interpenetrating fashion, These, in turn, enhance the GFA and strength of $Cu_{47.5}Zr_{47.5}Al_5$. However, compared to Cu-(0, 0, 12, 0), Al-(0, 0, 12, 0) in $Cu_{47.5}Zr_{47.5}Al_5$, owing to their Cu-lean shell configuration, have a comparatively lower tendency to form medium-range structures as determined by the ICOIs with different N values. Therefore, despite the larger number of (0, 0, 12, 0) in $Cu_{47.5}Zr_{47.5}Al_5$, Al-(0, 0, 12, 0) and the corresponding ICOIs in this alloy are structurally less stable. This makes them more susceptible to disordering. During disordering, these Al-(0, 0, 12, 0) underwent preferential disruption which occurred uniformly throughout the entire volume of the sample. As a result, the degree of softening associated with the disruption of ICOIs in $Cu_{47.5}Zr_{47.5}Al_5$ is less pronounced and is likely to result in less obvious strain localization. Therefore, $Cu_{47.5}Zr_{47.5}Al_5$, even though it is characterized by an extensive medium-range structure, can accommodate large plastic strains through spread-out shear transformations.

Acknowledgements

J.C. is grateful to Professor E. Ma at The Johns Hopkins University and Dr. Y.Q. Cheng at Oak Ridge National Laboratory for the valuable discussion and advice made throughout the present study conducted during his sabbatical leave in 2011. The major part of the present computation was carried out using the Grand Cluster Supercomputer at KIST. This work was supported by the Mid-career Researcher Program through an NRF (Grant No. 2009-0081023) funded by the MEST, Republic of Korea.

Appendix A. Quantification of a spatial distribution

A.1. Definition of the local inhomogeneity parameter

In order to quantify the degree of inhomogeneity of the spatial distribution of atoms, we employed the inhomogeneity parameter (h value) ordinarily used in wireless-network science [56]. Schilcher et al. attempted to quantify the spatial distribution of nodes distributed in two-dimensional (2-D) wireless networks [56]. We extended their concept of describing the inhomogeneity of nodes in a 2-D wireless network into 3-D space in order to quantify the spatial distribution of specific atoms in glassy structures. First, a given 3-D space (or calculation box) was divided into subvolumes of the same size. This was done by dividing three edges of the box into n segments of the same length so that the volume of the box is subdivided into the n^3 rectangular parallelepiped subvolumes (termed "grids"). Each grid can contain different numbers of atoms, which is termed m_i with i being the grid number. When N atoms are distributed uniformly with an equal spacing in the box, the mean number ($\bar{m}(n^3)$) of atoms calculated for n^3 grids is given by:

$$\bar{m}(n^3) = \frac{N}{n^3}. \tag{1}$$

In this case, the mean value ($\bar{m}$) and the actual number of atoms (m_i) in each grid are equal. However, in a system with non-uniform distribution of atoms, the values of $\bar{m}$ and m_i are not the same. This difference between $\bar{m}$ and m_i provides the basis for quantifying the local inhomogeneity of the spatial distribution of atoms. With this in mind, one can define the inhomogeneity parameter $\hat{h}$, which quantifies the degree of inhomogeneity of the spatial distribution of atoms, by adding all the differences between $\bar{m}$ and m_i.

$$\hat{h}(n^3) = \sum_{i=1}^{n^3} \left| m_i - \bar{m}(n^3) \right|. \tag{2}$$

At this point, we consider the two extreme cases to observe the range of the values of $\hat{h}$ in a system, where grids are generated such that $N = n^3$. If atoms are distributed in a perfectly uniform manner, each grid contains exactly one atom and, thus, $\hat{h}$ will be 0 (because $\bar{m} = m_i = 1$). However, when all atoms are clustered at a point, these atoms will be positioned within a single grid no matter how small the grids are made. In this case, the value of $\hat{h}$ becomes a maximum and can be determined as:

$$\hat{h}(n^3) = 2N\left(1 - \frac{1}{n^3}\right). \tag{3}$$

Since the grids are so small (or equivalently, the number of grids is large), the term $1/n^3$ in Eq. (3) can be approximated to be 0, leading to $\hat{h} \approx 2N$. The result indicates that the value of $\hat{h}$ varies depending on the number of atoms considered in the analysis. In order to eliminate the dependence of $\hat{h}$ on N, $\hat{h}$ in Eq. (2) is normalized by division with $2N$, as shown in Eq. (4). This operation makes the value of $\hat{h}$ be independent of N and limits its value between 0 and 1.

$$\hat{h}(n^3) = \frac{1}{2N} \sum_{i=1}^{n^3} \left| m_i - \bar{m}(n^3) \right|. \tag{4}$$

High $\hat{h}$ values as evaluated by Eq. (4) indicate an inhomogeneous distribution of atoms, whereas low values represent a homogeneous distribution. However, when $\hat{h}$ is evaluated using Eq. (4) for the two different systems with the different degrees of inhomogeneity, the difference in the $\hat{h}$ values corresponding to the two systems varies depending on the grid number generated in the box [56]. This dependence of the $\hat{h}$ value on the grid number was eliminated by incorporating a weighted-sum technique [57], in which larger number of grids take a lower weight and vice versa [56]. For this purpose, the edges of the 3-D box were divided into $2, 4, 8, \ldots, 2^r$ segments of the same length, and, thus, the corresponding numbers of grids were $2^3, 4^3, 8^3, \ldots, 2^{3r}$, where r is chosen such that each grid contains at most one atom. By incorporating the weight factor w in Eq. (4) and following the weighted-sum technique, the inhomogeneity parameter h can be written as Eq. (5).

$$h \equiv \sum_{k=1}^{r} w^{1-k}\hat{h}(2^{3k}) \tag{5.1}$$

$$= \frac{1}{2N}\sum_{k=1}^{r} w^{1-k}\sum_{i=1}^{2^{3k}}\left|m_i - \bar{m}(2^{3k})\right|. \tag{5.2}$$

The weight factor w in Eq. (5) assigns a weight to the inhomogeneity parameter $\hat{h}$ according to the segment number of the box (now, 2^k in Eq. (5)), and renders the resultant h value independent on the number of grids. In this study, we chose the value of w such that the value of h lies between 0 and 1. This was achieved by considering the two distribution configurations; when atoms are distributed in a completely uniform manner, the value of h will be 0, regardless of the weight factor w (because $\bar{m} = m_i$). In contrast, when atoms are clustered at a point, the values of h will vary according to the value of w. In order to limit the value of h to a maximum of 1, the value of w was determined by substituting Eq. (3) to Eq. (5) followed by setting $h = 1$. These calculation procedures are given in Eq. (6), and the result is $w \approx 8.89$. Once the value of w is determined, the value of h can now be evaluated using Eq. (7).

$$h = \sum_{k=1}^{\infty} w^{1-k}\left(1 - \frac{1}{2^{3k}}\right) = \sum_{k=1}^{\infty} w^{1-k} - \sum_{k=1}^{\infty}\frac{w^{1-k}}{2^{3k}}$$
$$= \frac{w}{w-1} - \frac{w}{8w-1} = 1. \tag{6}$$

$$h = \frac{1}{2N}\sum_{k=1}^{r} 8.89^{1-k}\sum_{i=1}^{2^{3k}}\left|m_i - \bar{m}(2^{3k})\right|. \tag{7}$$

A.2. Verification of the inhomogeneity parameter in various configurations

The validity of the proposed parameter was tested by calculating the h values for the 3-D boxes containing atoms with different degrees of inhomogeneity as shown in Fig. A1. In these figures, only atoms on a thin plane are shown to better illustrate their distribution. In the case of the box where atoms are positioned at the exact lattice points of a simple cubic structure (Fig. A1a), h was calculated as 0.02, which is close to 0. With an increasing degree of inhomogeneity (Fig. A1b–i), h values also increased and approached 0.99, which is the number close to the theoretical maximum value of 1, when atoms are clustered together.

The h value must be independent of the linear operations of distributed atoms, e.g. translation and rotation. This was tested here by comparing the h value of the original distribution with those calculated for the configurations generated by translation and rotation. Fig. A2 shows images of the atomic distributions ($h = 0.49$) generated by translation and rotation of the original distribution. Even if the atoms in the 3-D box are reproduced by translation and rotation, the corresponding h values are the same as that for the original configuration. Therefore, we believe that the equation derived here is appropriate to quantify the inhomogeneity of the spatial distribution of atoms.

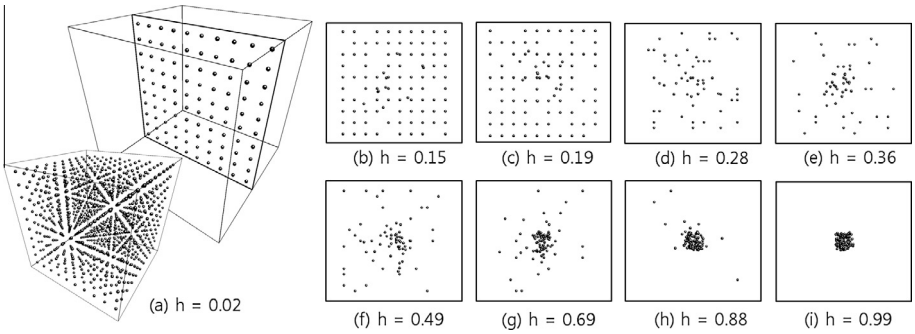

Fig. A1. Spatial distributions of atoms with different degrees of inhomogeneity and corresponding h values: (a) $h = 0.02$, (b) $h = 0.15$, (c) $h = 0.19$, (d) $h = 0.28$, (e) $h = 0.36$, (f) $h = 0.49$, (g) $h = 0.69$, (h) $h = 0.88$ and (i) $h = 0.99$.

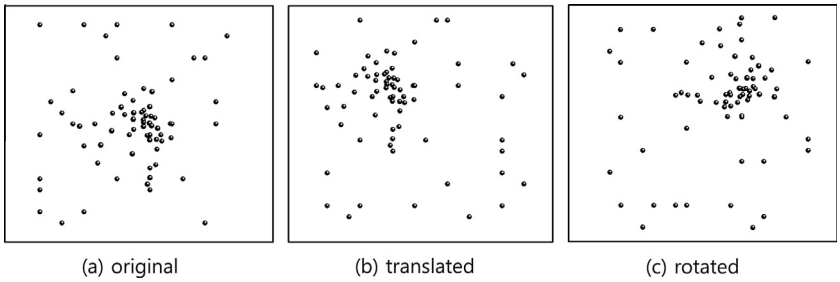

Fig. A2. Spatial distributions of atoms with $h = 0.49$: (a) original distribution is (b) translated and (c) rotated in the periodic condition.

References

[1] Sheng HW, Cheng YQ, Lee PL, Shastri SD, Ma E. Acta Mater 2008;56:6264.
[2] Yang L, Jiang JZ, Liu T, Hu TD, Uruga T. Appl Phys Lett 2005;87:061918.
[3] Shi Y, Falk ML. Phys Rev B 2006;73:214201.
[4] Wakeda M, Shibutani Y, Ogata S, Park J. Intermetallics 2007;15:139.
[5] Lee J-C, Park K-W, Kim K-H, Fleury E, Lee B-J, Wakeda M, et al. J Mater Res 2007;22:3087.
[6] Park K-W, Jang J-i, Wakeda M, Shibutani Y, Lee J-C. Scripta Mater 2007;57:805.
[7] Cheng YQ, Cao AJ, Sheng HW, Ma E. Acta Mater 2008;56:5263.
[8] Shi Y, Falk ML. Phys Rev Lett 2005;95:095502.
[9] Cheng YQ, Ma E, Sheng HW. Phys Rev Lett 2009;102:245501.
[10] Cao QP, Li JF, Zhou YH, Jiang JZ. Scripta Mater 2008;59:673.
[11] Eckert J, Das J, Kim KB, Baier F, Tang MB, Wang WH, et al. Intermetallics 2006;14:876.
[12] Lee S-W, Huh M-Y, Fleury E, Lee J-C. Acta Mater 2006;54:349.
[13] Cheng YQ, Cao AJ, Ma E. Acta Mater 2009;57:3253.
[14] Lee M, Lee C-M, Lee K-R, Ma E, Lee J-C. Acta Mater 2011;59:159.
[15] Miracle DB. Nat Mater 2004;3:697.
[16] Sheng HW, Luo WK, Alamgir FM, Bai JM, Ma E. Nature 2006;439:419.
[17] Wang XD, Yin S, Cao QP, Jiang JZ, Franz H, Jin ZH. Appl Phys Lett 2008;92:011902.
[18] Wang SY, Wang CZ, Li MZ, Huang L, Ott RT, Kramer MJ, et al. Phys Rev B 2008;78:184204.
[19] Hufnagel TC, Brennan S. Phys Rev B 2003;67:014203.
[20] Fan C, Wilson TW, Dmowski W, Choo H, Richardson JW, Maxey ER, et al. Intermetallics 2006;14:888.
[21] Hui X, Gao R, Chen GL, Shang SL, Wang Y, Liu ZK. Phys Lett A 2008;372:3078.
[22] Hui X, Fang HZ, Chen GL, Shang SL, Wang Y, Qin JY, et al. Acta Mater 2009;57:376.
[23] Baser TA, Das J, Eckert J, Baricco M. J Alloys Compd 2009;483:146.
[24] Sarmah R, Ananthakrishna G, Sun BA, Wang WH. Acta Mater 2011;59:4482.
[25] Song KK, Pauly S, Zhang Y, Scudino S, Gargarella P, Surreddi KB, et al. Intermetallics 2011;19:1394.
[26] Pauly S, Liu G, Gorantla S, Wang G, Kühn U, Kim DH, et al. Acta Mater 2010;58:4883.
[27] Hoover WG. Phys Rev A 1985;31:1695.
[28] Hoover W. Phys Rev A 1986;34:2499.
[29] Park K-W, Lee C-M, Wakeda M, Shibutani Y, Falk ML, Lee J-C. Acta Mater 2008;56:5440.
[30] EPAPS Document No. E-PRLTAO-103-011927. For more information on EPAPS, see <http://www.aip.org/pubservs/epaps.html>.
[31] Chen H, Waseda Y. Phys Status Solid A 1979;51:593.
[32] Bionducci M, Buffa F, Licheri G, Navarra G, Bouchet-Fabre B, Tonnerre J. J Phys Sci 1996;51:71.
[33] Mattern N, Schöps A, Kühn U, Acker J, Khvostikova O, Eckert J. J Non-Cryst Solids 2008;354:1054.
[34] Kim YM, Lee BJ. J Mater Res 2008;23:1095.
[35] Sadoc A, Calvayrac Y, Quivy A, Harmelin M, Flank A. J Non-Cryst Solids 1984;65:109.
[36] Babanov YA, Schvetsov V, Sidorenko A. Physica B 1995;208:375.
[37] Pduraru A, Kenoufi A, Bailey NP, Schiøtz J. Adv Eng Mater 2007;9:505.
[38] Duan G, Xu D, Zhang Q, Zhang G, Cagin T, Johnson WL, et al. Phys Rev B 2005;71:224208.
[39] Miracle D, Sanders W, Senkov O. Philos Mag 2003;83:2409.
[40] Wang ZT, Zeng KY, Li Y. Scripta Mater 2011;65:747.
[41] Peng HL, Li MZ, Wang WH, Wang CZ, Ho KM. Appl Phys Lett 2010;96:021901.
[42] Sha ZD, Feng YP, Li Y. Appl Phys Lett 2010;96:061903.
[43] Fang HZ, Hui X, Chen GL, Liu ZK. Appl Phys Lett 2009;94:091904.
[44] Wakeda M, Shibutani Y. Acta Mater 2010;58:3963.
[45] Lee C-M, Park K-W, Lee B-J, Shibutani Y, Lee J-C. Scripta Mater 2009;61:911.
[46] Shimono M, Onodera H. Mater Sci Forum 2007;539:2031.
[47] Mendelev MI, Kramer MJ, Ott RT, Sordelet DJ, Besser MF, Kreyssig A, et al. Philos Mag 2010;90:3795.
[48] Nelson DR, Spaepen F. Solid State Phys 1989;42:1.
[49] Widom M, Al-Lehyani I, Moriarty JA. Phys Rev B 2000;62:3648.
[50] Park K-W, Lee C-M, Lee M-R, Fleury E, Falk ML, Lee J-C. Appl Phys Lett 2009;94:021907.
[51] Shi Y, Katz MB, Li H, Falk ML. Phys Rev Lett 2007;98:185505.
[52] Lee S-C, Lee C-M, Yang J-W, Lee J-C. Scripta Mater 2008;58:591.
[53] Manning M, Daub E, Langer J, Carlson J. Phys Rev E 2009;79:016110.
[54] Manning M, Langer J, Carlson J. Phys Rev E 2007;76:056106.
[55] Park K-W, Shibutani Y, Falk ML, Lee B-J, Lee J-C. Scripta Mater 2010;63:231.
[56] Schilcher U, Gyarmati M, Bettstetter C, Chung YW, Kim YH. Vehicular Technology Conference (VTC) Spring 2008;2008:2690.
[57] Grossman J., Grossman M., Katz R. The first systems of weighted differential and integral calculus. Massachusetts: Archimedes Foundation; 1980.